INTERNATIONAL JOURNAL OF MICROWAVE AND OPTICAL TECHNOLOGY
VOL.21, NO.1, JANUARY 2026

Modeling and Experimental Study of Loudspeaker Directivity Patterns in the Far and Near Fields

Islam J. Islamov[1], Kalin S. Kalinov[2], Iliyan Y. Iliev[3], Ramil G. Akhundov[4], Vagif A. Gasimov[5], Boyan K. Mednikarov[6], Miroslav Y. Tsvetkov[7]

[1]Department of Automation, Telecommunications and Energy, Baku Engineering University, Hasan Aliyev str., 120, AZ0101, Baku, Azerbaijan
isislamov@beu.edu.az
[2,3,6,7]Faculty of Engineering, Nikola Vaptsarov Naval Academy, 73 Vasil Drumev Street, 9002, Varna, Bulgaria
k.kalinov@nvna.eu; i.y.iliev@naval-acad.bg; rector@naval-acad.bg; m.tsvetkov@naval-acad.bg
[4]Military Scientific Research Institute, National Defense University, Golden East 13, AZ1065, Baku, Azerbaijan
mr.axundov1@gmail.com
[5]Faculty of Information and Computer Technologies, Baku Engineering University, Hasan Aliyev str., 120, AZ0101, Baku, Azerbaijan
vaqasimov@beu.edu.az

Abstract **- The current paper reviews theoretically and examines experimentally the polar plot of a loudspeaker in the far and near field. An original equation for sound pressure calculation in the near and far field is proposed. An experiment is conducted to confirm the theoretical data and the accuracy of the proposed expression. Several conclusions are drawn from the analysis of the study. Sound emission from a linear array of loudspeakers, whose excitation factors are set in accordance with the Bessel functions, creates a sound pressure distribution in the plane of the loudspeaker axes that corresponds to the radiation pattern of a single loudspeaker. Experimental data confirms that the Bessel array's directivity pattern broadens compared to a linear array of loudspeakers with a constant excitation factor, and approaches that of a single loudspeaker. Considering the analyzed patterns in selecting the number of loudspeakers is recommended when designing Bessel arrays to create an omnidirectional sound pressure distribution with an overall increase in sound pressure level. The novelty and originality of this work lies in its ability to more accurately determine the fundamental resonance frequency of a loudspeaker's moving system, establish the optimal amplifier output stage load and crossover filter element data, and also improve the frequency range, rated power, and sensitivity.**

Index Terms **- Mathematical Modeling, Loudspeaker, Polar Plot, Near Field, Far Field, Sound Pressure, Measurements.**

I. INTRODUCTION

The widespread use of loudspeakers in commercial and defense applications means that engineers with only a passing familiarity with their operating principles are often entrusted with these designs. The term “loudspeaker”, like the design itself, is far from new; their theoretical foundations have been developed over several decades, but most existing publications are primarily aimed at specialists well versed in mathematical analysis and electromagnetic fields.

As loudspeakers are increasingly used in mixed-signal systems, many designers would appreciate a simple explanation of the concepts and principles of their polar patterns. As it turns out, there are many analogies between loudspeaker behavior and the time-sampling systems that mixed-signal engineers encounter almost daily. This article is not intended for loudspeaker design engineers; rather, it aims to assist designers working with subsystems or components used in loudspeakers. This article will help to some extent visualize the principles that determine how an engineer's actions can affect the loudspeaker's directivity pattern.

The controlling and modeling of loudspeakers and microphones’ radiation pattern has become a

INTERNATIONAL JOURNAL OF MICROWAVE AND OPTICAL TECHNOLOGY
VOL.21, NO.1, JANUARY 2026

separate scientific branch of acoustics. Through deeper understanding of the problem's nature the examination and improvement of microphones' radiation has become possible [1, 2], as well as the manufacturing of directed [3, 4] and hyper directed loudspeakers [5-7]. When directed sound pressure is generated by powerful sound waves, one can overcome the gravitational force [8-11] or excite liquid, during which process, short bursts of light are emitted [12-15]. That process is called sonoluminescence. During sonoluminescence sound waves form little bubbles in the liquid, that bloat and implode quickly, which results in producing light. At the same time huge amount of heat is released. Directed microphones and loudspeakers are often used in architectural acoustics as well [16-20].

In the present paper the radiation pattern of a circular piston in the near [7] and far [8] field is theoretically reviewed and experimentally examined.

II. THEORETICAL BACKGROUND

The object of this study is a circular piston. Due to its symmetry with respect to the *z* axis (Fig. 1) one can assume that its polar pattern will be one with rotational symmetry.

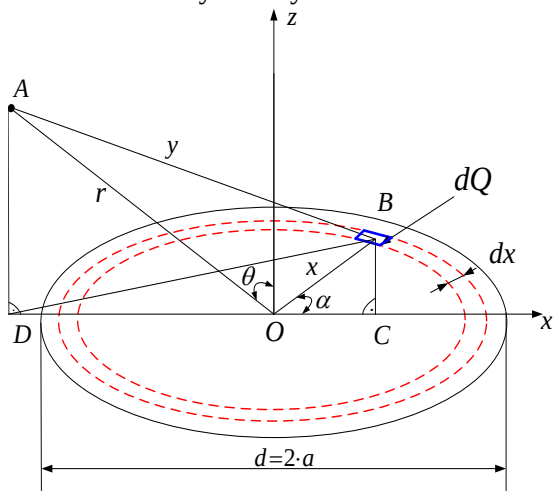

Fig. 1. Geometry of a circular piston directivity [21].

To define that symmetry, it is sufficient to determine the sound pressure level at distance r in a plane who's normal is perpendicular to the z axis.

The sound pressure created by the emitter in the environment can be calculated under the assumption that its surface consists of multiple elementary sections dQ. The surface area of each elementary section can be determined using the following relation [22-25]:

$$dQ = x \cdot dx \cdot d\alpha. \quad (1)$$

Each of the elementary section creates sound pressure in point *A*. Point *A* is situated at distance y and angle θ with respect to the z axis. The sound pressure is [26-29]:

$$dp_\theta = \frac{r_0 p_m}{y} e^{j(\omega t - ky)}, \quad (2)$$

where y is the distance between the elementary section and point *A* (Fig. 1); p_m – the instantaneous amplitude of the sound pressure; r_0– the radius of the point section.

With reference to Fig. 1 where angle *DCB* = 90º one can derive several expressions:

$$\overline{DC} = \overline{DO} + \overline{OC} = r\sin\theta + x\cos\alpha; \quad (3)$$

$$\overline{BD^2} = \overline{DC^2} + \overline{CB^2} = (rsin\theta + xcos\alpha)^2 + \\ +x^2 sin^2\alpha = r^2 sin^2\theta + 2rx\theta cos\alpha + x^2, \quad (4)$$

$$\overline{AB^2} = \overline{BD^2} + \overline{AD^2} = r^2 sin^2\theta + \\ +2rxsin\theta cos\alpha + x^2 + r^2 cos^2\theta. \quad (5)$$

Equation (5) can also be represented as:

$$y^2 = r^2 + x^2 + 2rx\sin\theta\cos\alpha \quad (6)$$

or

$$y = \sqrt{r^2 + x^2 + 2rx\sin\theta\cos\alpha}. \quad (7)$$

Instantaneous amplitude of the sound pressure is [30-33]:

$$p_m = \rho_s c_0 k r_0 v_m. \quad (8)$$

where c_0 is a speed of sound; $k = \frac{2\pi}{\lambda}$– wave number; v_m– particles velocity; ρ_s – density of the environment; λ – wave length.

After multiplying both sides of the expression (8) by r_0, and also multiplying the right-hand side by $\frac{2\pi}{2\pi}$ one can take into consideration that the surface of the point emitter is $2\pi r_0^2 = dQ$ and subsequently:

$$r_0 p_m = \frac{\rho_s c_0 k v_m}{2\pi} dQ. \quad (9)$$

If expressions (1) and (9) are substituted in equation (2), the elementary sound pressure in the direction defined by the θ angle will be as follows:

$$dp_\theta = \frac{\rho_s c_0 k v_m}{2\pi y} e^{j(\omega t - ky)} x dx d\alpha. \quad (10)$$

After expression (7) is substituted in the previous equation (10) and it is afterwards applied to the entire surface of the piston, the following original equation for calculating the total sound pressure level, created by all point emitters, can be rewritten:

$$p_\theta = \frac{\rho_s c_0 k v_m}{2\pi} e^{j\omega t} \times \times \int_0^a x dx \int_0^{2\pi} \frac{e^{-jk\left(\sqrt{r^2+x^2+2rx\sin\theta\cos\alpha}\right)}}{\sqrt{r^2+x^2+2rx\sin\theta\cos\alpha}} d\alpha. \quad (11)$$

For the far field, when the distance is significantly larger than the diameter of the piston ($r >> d$), the denominator of the integrant is $\sqrt{r^2 + x^2 + 2rx\sin\theta\cos\alpha} = r$ (Fig. 2), and the numerator is $e^{-jk\left(\sqrt{r^2+x^2+2rx\sin\theta\cos\alpha}\right)} = e^{-jk(r+x\sin\theta\cos\alpha)}$ (Fig. 3).

After the new denominator and numerator are replaced in expression (11), the well-known expression for calculating sound pressure level, created by all point emitters, can be rewritten [34-37]:

$$p_\theta = \frac{\rho_s c_0 k v_m}{2\pi r} e^{j\omega t} \times \times \int_0^a x dx \int_0^{2\pi} e^{-jk(r+x\sin\theta\cos\alpha)} d\alpha. \quad (12)$$

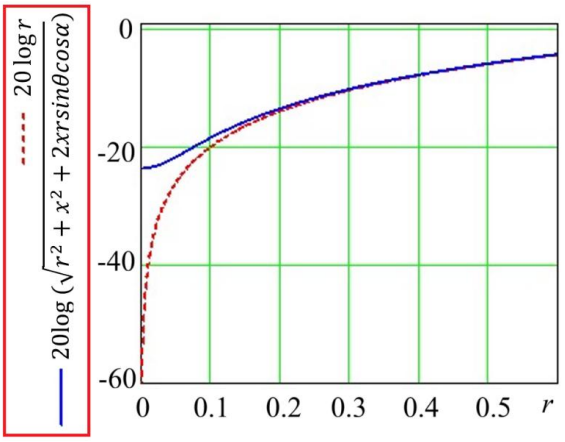

Fig. 2. Graphic representation of the denominators in the newly-proposed original expression (11) – solid blue line and the well-known expression (12) – dashed red line.

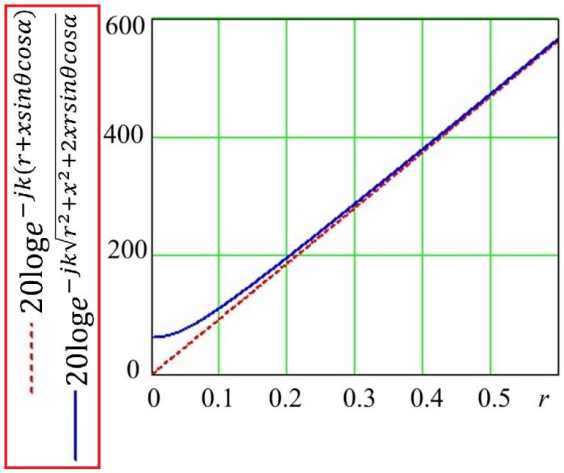

Fig. 3. Graphic representation of the numerators in the newly-proposed original expression (11) – solid blue line and the well-known expression (12) – dashed red line.

After integrating by α, expression (12) becomes [38-40]:

$$p_\theta = \frac{\rho_s c_0 k v_m}{r} e^{-jkr} \int_0^a J_0(kx\sin\theta) x dx, \quad (13)$$

where $J_0(kx\sin\theta)$ is Bessel function of the zero kind of the argument $(kx\sin\theta)$, and after integrating by x, one obtains [41, 42]:

$$p_\theta = \frac{\rho_s c_0 k v_m a^2}{r} e^{-jkr} \frac{J_1(kasin\theta)}{kasin\theta}, \quad (14)$$

where $J_1(kasin\theta)$ is Bessel function of the first kind of the argument $(kasin\theta)$.

The Bessel function can also be represented as [14]:

$$J_1(kasin\theta) = \frac{kasin\theta}{2} - \frac{k^3 a^3 sin^3\theta}{2^2 4} + \\ + \frac{k^5 a^5 sin^5\theta}{2^2 4^2 6} - \cdots, \quad (15)$$

therefore, the interrelation after the e^{-jkr} in expression (14) can be rewritten [9]:

$$\frac{J_1(kasin\theta)}{kasin\theta} = \frac{1}{2} - \frac{k^2 a^2 sin^2\theta}{2^2 4} + \frac{k^4 a^4 sin^4\theta}{2^2 4^2 6} - \cdots \quad (16)$$

The radiation pattern $G(\theta)$ is derived from the interrelation [11]:

$$G(\theta) = \frac{p_\theta}{p_{0^\circ}}, \quad (17)$$

where p_{0° is the amplitude of the sound pressure level at the acoustic axis.

To obtain a radiation pattern it is necessary to determine the sound pressure level for $\theta = 0^\circ$. Due to the zero value of the θ angle, the expression (16) becomes:

$$\frac{J_1(kasin0^\circ)}{kasin0^\circ} = \frac{1}{2}, \quad (18)$$

and for the sound pressure level in that direction the following is valid:

$$p_{0^\circ} = \frac{\rho_s c_0 k v_m a^2}{r} e^{-jkr} \frac{1}{2}. \quad (19)$$

If expressions (14) and (19) are substituted in equation (17), the polar response of a circular piston in the far field will be:

$$G(\theta) = 2 \frac{J_1(kasin\theta)}{kasin\theta}. \quad (20)$$

There are zeros to be expected in the radiation pattern, when $k \cdot a \cdot \sin\theta$ is a root of Bessel function: 3.83 – Fig. 4; 7.02 – Fig. 5; 10.2 – Fig. 6; 13.3 – Fig. 7; 16.5.

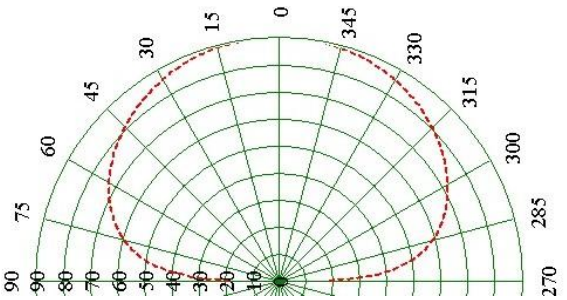

Fig. 4. Polar response at: $k \cdot a \cdot \sin\theta = 3.83$.

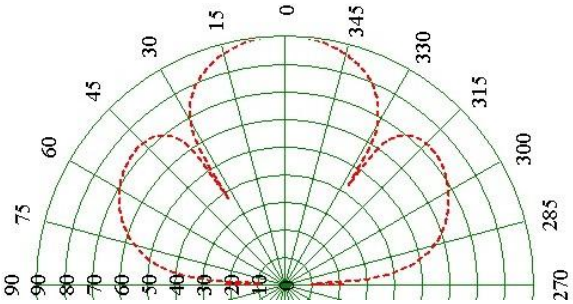

Fig. 5. Polar response at: $k \cdot a \cdot \sin\theta = 7.02$.

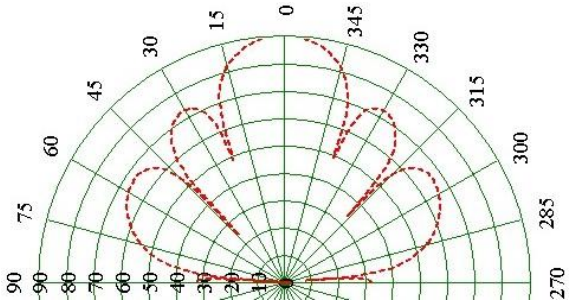

Fig. 6. Polar response at: $k \cdot a \cdot \sin\theta = 10.2$.

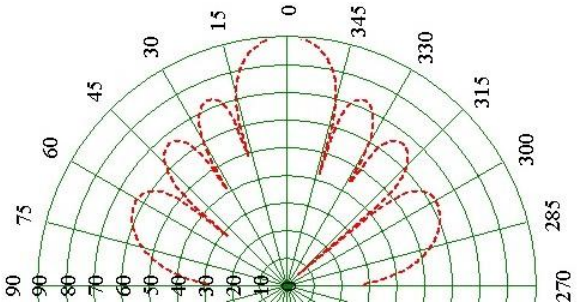

Fig. 7. Polar response at: $k \cdot a \cdot \sin\theta = 13.3$.

In Figs. 8-10 comparison is made between the newly-proposed original expression (11) and the well-known expression (12) for different distances and $k{\cdot}a{\cdot}sin\theta = 7.02$.

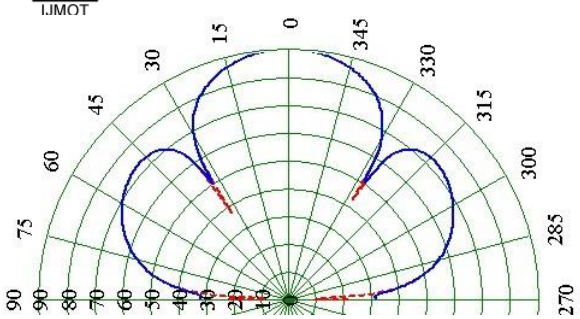

Fig. 8. Polar response at 2.40 *m* and $k \cdot a \cdot \sin\theta = 7.02$: solid blue line – newly-proposed original expression (11); dashed red line – well-known expression (12).

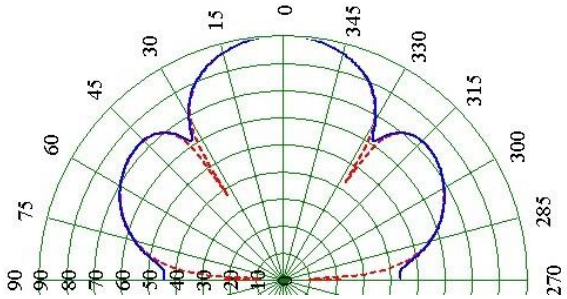

Fig. 9. Polar response at 0.60 *m* and $k \cdot a \cdot \sin\theta = 7.02$: solid blue line – newly-proposed original expression (11); dashed red line – well-known expression (12).

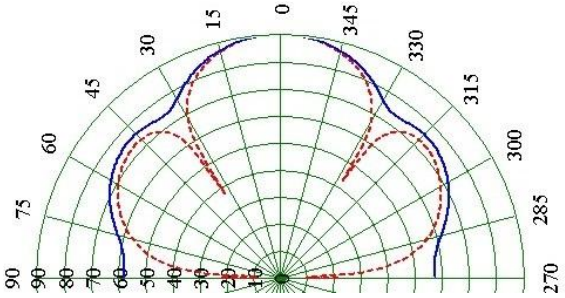

Fig. 10. Polar response at 0.15 *m* and $k \cdot a \cdot \sin\theta = 7.02$: solid blue line – newly-proposed original expression (11); dashed red line – well-known expression (12).

III. EXPERIMENTAL SETUP AND RESULTS

The practical measurements were carried out with a sound-level meter Robotron Präzisions, a microphone MK301, a sound card Realtek High-Definition Audio and a Matlab® program [15] using a time selection method [16]. The object of the study is a JBL loudspeaker with nominal diameter of 0.13 *m*. The parameters were selected so that $k \cdot a \cdot \sin\theta = 7.02$.

Results from the measurements at different distances – 2.40 *m*, 0.60 *m* and 0.15 *m* from the loudspeaker are visually represented in Fig. 11, Fig. 12, Fig. 13.

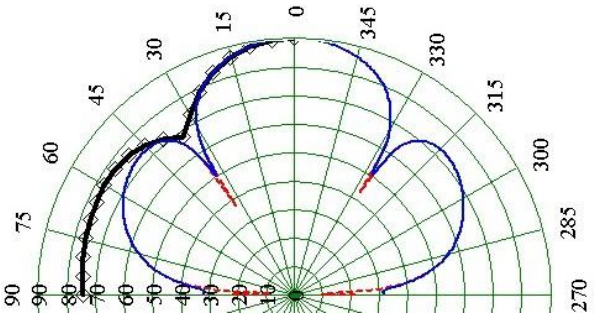

Fig. 11. Polar response at 2.40 *m* from the loudspeaker and $k \cdot a \cdot \sin\theta = 7.02$: solid blue line – newly-proposed original expression (11); dashed red line – well-known expression (12); solid black line with diamonds – experimental data (0º ÷ 90º).

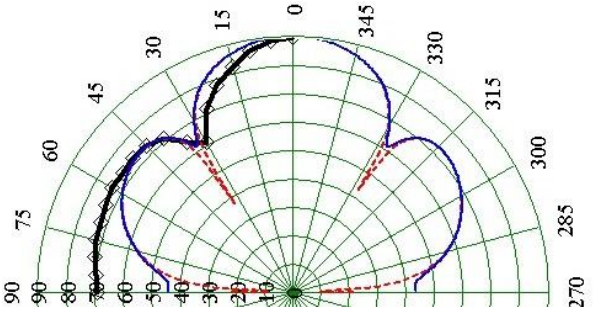

Fig. 12. Polar response at 0.60 *m* from the loudspeaker and $k \cdot a \cdot \sin\theta = 7.02$: solid blue line – newly-proposed original expression (11); dashed red line – well-known expression (12); solid black line with diamonds – experimental data (0º - 90º).

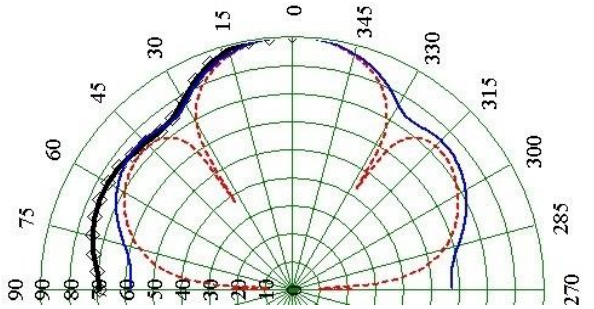

Fig. 13. Polar response at 0.15 *m* from the loudspeaker and $k \cdot a \cdot \sin\theta = 7.02$: solid blue line – newly-proposed original expression (11); dashed red line – well-known expression (12); solid black line with diamonds – experimental data (0º - 90º).

INTERNATIONAL JOURNAL OF MICROWAVE AND OPTICAL TECHNOLOGY
VOL.21, NO.1, JANUARY 2026

IV. EQUIVALENT CIRCUIT OF A LOUDSPEAKER

To construct a loudspeaker equivalent circuit, we don't need much: just get real-world equivalent circuits of the loudspeakers, i.e., those that take the acoustic design into account, run them in any simulator, and then run the calculated filters through it, but this time taking into account the actual load. Then, let loose, adjusting the filter element values, achieving brilliant results, and always remaining energized. The result may not be 100% accurate, but it will be significantly closer to real life than if filters were designed without taking the actual complex load into account. The equivalent circuit of the loudspeaker is shown in Fig. 14.

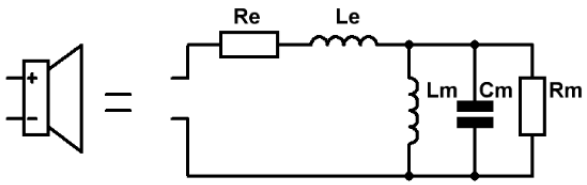

Fig. 14. The equivalent circuit of the loudspeaker.

Where, R_e and L_e are the resistance and inductance of the voice coil (specified in the datasheet, but can be easily measured with standard instruments). These elements cause the speaker's impedance to increase in the high-frequency range of frequencies applied to it. In the case shown in Fig. 14, this increase is noticeable starting at 100 *Hz*.

The parallel resonant circuit formed by L_m, C_m, and R_m forms an electrical circuit that simulates the mechanical properties of a loudspeaker, i.e., its ability to resist cone movement. In Fig. 14, this circuit leads to a resonant surge in the speaker's impedance around 33 *Hz*. Since L_m = 12.46 *mH*, C_m=1868 μF, R_m = 44 *Ohm*. R_e (voice coil DC resistance) – 4.1 *Ohm*, L_e (voice coil inductance) – 2.6 *mH*. F_s (natural resonant frequency) – 33 *Hz*, Q_{ms} (mechanical quality factor) – 6.84, Q_{es} (electrical quality factor) – 0.63, Q_{ts} (total quality factor) – 0.57. A comparison of the results of existing works and this work on loudspeaker parameters is shown in Table 1.

Table 1: Comparison of the results of existing works and this work on loudspeaker parameters.

References	Frequency band, *Hz*	Nominal power, *W*	Characteristic sensitivity level, *dB*
[5]	60-15 500	50	75
[6]	50-14 500	60	65
[7]	75-14 500	40	85
[8]	20-15000	45	75
[9]	20-20000	50	90
This work	30-30000	75	100

The frequency response of a loudspeaker's impedance allows for a more accurate determination of the fundamental resonance frequency of the loudspeaker's moving system, the optimal amplifier output stage load, and the crossover filter element data. Table 1 demonstrates that the voice coil's active impedance alone should not be used in calculating the amplifier's load. The average absolute value of the voice coil's impedance will obviously be its value at 1.5 or 2.5 *kHz*, depending on the higher cutoff frequency. It is also important to consider whether an increase in load resistance versus the nominal value is more undesirable in terms of increased distortion for the amplifier being used. The calculated value should be selected based on this and the frequency response of the loudspeaker's impedance. When calculating the crossover filter, the average absolute value of the loudspeaker's impedance over its operating frequency band (the filter's transparency band). As can be seen from Table 1, this system allows for a more accurate determination of the fundamental resonance frequency of the loudspeaker's moving system, the optimal amplifier output stage load, and the crossover filter element data, as well as an improved frequency response, rated power, and sensitivity.

V. CONCLUSION

A study of the well-known expression (20) for far field polar response calculation reveals several conclusions: the polar pattern form depends on the relation between the loudspeaker’s diameter (respectively radius a) and the emitted sound wave’s length (wave number *k*); when the size of the loudspeaker is significantly smaller than the emitted wave length, then the and $G(\theta) \approx 1$.

From the experimental data analysis of the expressions (11) and (12) and their graphic representation (Figs. 11-13), one can deduce: the newly-proposed, by the author generalized expression for sound pressure level calculation (11) is more accurate compared to the well-known expression (12) in regards to the near field and hence it should be used for determining the sound pressure level in it; practically, in the space directly in front of the loudspeaker the radiation pattern lacks pronounced minimums, while in the far field the minimums become commeasurable with the measuring system's (microphone, sound card) proper noises; the greater the distance the more the graphic representation of the two expressions – the one proposed by the author (11) and the well-known (12) – over lapses and in the far field it becomes completely identical.

ACKNOWLEDGMENT

The authors express their deep gratitude to the entire editorial board of the journal for their professionalism and excellent work. I especially want to note the very careful and attentive attitude of the reviewers, and their detailed study of the manuscript of the article. Their comments and recommendations are constructive, which allows for improving the quality of the presented research and structuring of the article as much as possible according to the requirements of the journal. The friendly and prompt nature of communication with the editorial board contributes to the rapid resolution of all emerging issues and compliance with the stated deadlines for reviewing and publishing the article. This publication was carried out under project G7475, funded by the NATO Science for Peace and Security Programmed.

REFERENCES

[1] R.P.M. Thomas, J. Ahrens, and I.J. Tashev, "Beamformer Design Using Measured Microphone Directivity Patterns: Robustness to Modelling Error," *Proceedings of The 2012 Asia Pacific Signal and Information Processing Association Annual Summit and Conference*, Hollywood, CA, USA, pp. 1-4, 2012.

[2] I. Tashev, "Robust design of wideband loudspeaker arrays," *Acoustics, Speech and Signal Processing*, pp. 1-5, 2009.

[3] G. Woon-Seng, J. Yang, and T. Kamakura, "A review of parametric acoustic array in air," *Applied Acoustics*, vol. 73(12), pp. 1211-1219, 2012.

[4] J.R. Wu, "Acoustical tweezers," *The Journal of the Acoustical Society of America*, vol. 89(5), pp. 2140-2143, 1991.

[5] D.F. Gaitan, L.A. Crum, C.C. Church, and R.A. Roy, "Sonoluminescence and bubble dynamics for a single, stable, cavitation bubble," *The Journal of the Acoustical Society of America*, vol. 91(6), pp. 3166-3183, 1992.

[6] O. Warusfel, and N. Misdariis, "Directivity synthesis with a 3D array of loudspeakers-application for stage performance," *In Proceedings of the COST G-6 Conference on Digital Audio Effects*, Limerick, Ireland, pp. 1-5, 2001.

[7] I. Iliev, E. Sirakov, and H. Zhivomirov, "Sound near field examination of circular piston," *Conference Proceedings*, II, II-59–II-63, 2013.

[8] E. Sirakov, "Polar diagram of multiple driver loudspeaker system," *Int. Scientific Conference of Information Communication*, vol. 1, pp. 317-320, 2007.

[9] I.S. Vahitov, "Theoretical principles of electroacoustics and electroacoustics devices, *Art*, pp. 411-413, 1982.

[10] L.E. Kinsler, A.R. Frey, A.B. Coppens, and J.V. Sanders, "Fundamentals of Acoustics," 4th ed., New York, John Wiley&Sons, 534 p., 2000.

[11] G.S. Genzel, and A.M. Zaiezdni, "Fundamentals of Acoustics," *Sea transport*, 388 p., 1952.

[12] L.L. Beranek, and T.J. Mellow, "Acoustics: Sound Fields and Transducer," *Academic Press*, 704 p., 2012.

[13] T.D. Rossing, M. Schroeder, W. Hartmann, N. Fletcher, F. Dunn, D. Campbell, and A. Pierce, "Springer Handbook of Acoustics," New York, 1167 p., 2007.

[14] I.S. Gradshteyn, and I.M. Ryzhik, "Table of integrals, series and product," Academic Press, 7th ed., London, Elsevier, 1161 p., 2007.

[15] H. Zhivomirov, and I. Iliev, "Radiation Pattern Measurement with Matlab Implementation," *Journal of the Technical University of Gabrovo*, vol. 52, pp. 73-76, 2016.

[16] H. Miller, "3-dimensional acoustic measurements using gating techniques," *Bruel&Kjaer Application notes*, pp. 17-163, 1976.

[17] I.J. Islamov, F.G. Agayev, and G.V. Aliyeva, "Electrodynamic Modeling of a Planar Antenna System for Wireless Communication," *Advanced Physical Research*, vol. 7(1), pp. 87-101, 2025.

[18] I.J. Islamov, R.G. Akhundov, D. Dimitrov, and V. Panevski, "Modeling of a Circular Disk Monopole Antenna Fed from a Microwave Broadband Coplanar Waveguide," *Advanced Physical Research*, vol. 7(2), pp. 184-195, 2025.

[19] W. Bhowmik, and S. Shweta, "Design of compact omnidirectional substrate integrated waveguide exponentially tapered multiple H-plane horn antenna," *AEU-International Journal of Electronics and Communications*, vol. 108, pp. 29-35, August 2019.

[20] L. Yu, G. Zixin, Y. Ningning, A. Wenxing, and M. Kaixue, "A Flat-Top Beam H-plane SIW Horn Antenna Based on Beamforming," *IEEE Antennas and Wireless Propagation Letters*, vol. 5, pp. 588-592, November 2023.

[21] Y. Ningning, J. Chuansheng, L. Yu, M. Kaixue, "Wideband and Miniaturized Phase-Corrected Empty Substrate-Integrated H-Plane Horn Antenna for 5G Millimeter Waves," *IEEE Transactions on Antennas and Propagation*, vol. 71(9), pp. 7638-7643, June 2023.

[22] W. Hong, "The role of millimeter-wave technologies in 5G/6G wireless communications," *IEEE J. Microw*., vol. 1(1), pp. 101-122, January 2021.

[23] L. Wang, M. Esquius-Morote, H. Qi, X. Yin, and J. R. Mosig, "Phase corrected H-plane horn antenna in gap SIW technology," *IEEE Trans. Antennas Propag*., vol. 65 (1), pp. 347-353, November 2017.

[24] J. Wang, F. Wu, , Z. H. Jiang, Y. Li, and D. Jiang, "A millimeter-wave substrate integrated waveguide H-plane horn antenna with enhanced gain and efficiency," *IEEE Antennas Wireless Propag. Lett*., vol. 21(4), pp. 769-773, January 2022.

[25] Y. Zhang, J. Deng, D. Sun, J. Yin, and L. Guo, "Compact slow-wave SIW H-plane horn antenna with increased gain for vehicular millimeter wave communication," *IEEE Trans. Veh. Technol*., vol. 70(7), pp. 7289-7293, June 2021.

[26] A. Amir, and S. Munkyo, "SIW Based D-Band Single and 2×2 MIMO Elliptically Tapered Slot Antenna," *IEEE Access*, vol. 11, pp. 87270-87278, August 2023.

[27] C. Ma, S. Ma, L. Dai, Q. Zhang, H. Wang and H. Yu, "Wideband and high-gain D-band antennas for next-generation short-distance wireless communication chips," *IEEE Trans. Antennas Propag*., vol. 69(7), pp. 3700-3708, July 2021.

[28] I. Muhammad, S. Kamel, T. M. Ahmed, M. Mahdi and A. Amin, "Wide-Angle Beam Steering Closed-Form Pillbox Antenna Fed by Substrate-Integrated Waveguide Horn for On-the-Move Satellite Communications. *Sensors*," vol. 24(3), 732-745, January 2024.

[29] U. Nissanov and G. Singh, "6G Broadband and High Directive Microstrip Antenna with SIW and FSSs," *Engineering Science and Technology*, vol. 5(1), pp. 1-16, Jule 2024.

[30] W. Shuqi, Z. Bin and F. Guangyou, "A Method for Low Sidelobe Substrate-Integrated Waveguide Slot Antenna Design Applied for Millimeter-Wave Radars," *Remote Sensing*, vol. 16(3), pp. 1-21, January 2024.

[31] I. A. Barannikov, K. A. Berdnikov, S. I. Derevyankin, E. A. Ishchenko, K. V. Smuseva, and S. M. Fyedorov, "Reflector antenna based on SIW technology," *Radio engineering and communications*, vol. 18(2), pp. 72-76, January 2022.

[32] M. Moradian, "Employing the dumbbell-shaped longitudinal slot antennas in the planar slotted antenna arrays," *International Journal of Microwave and Wireless Technologies*, vol. 14, no. 7, pp. 914-925, September 2022.

[33] G. Srivastava, B.K. Kanuijia and P. Rajeev, "UWB MIMO antenna with common radiator," *International Journal of Microwave and Wireless Technologies*, vol. 9, no. 3, pp. 573-580, April 2017.

[34] A. Basit, W.Q. Wang and S.Y. Nusenu, "Adaptive transmit beamspace design for cognitive FDA radar tracking," *Radar Sonar Navig*., vol. 13, no. 12, pp. 2083-2092, December 2019.

[35] H.K. Qasim, "Reconfigurable Compact Wide-Band Quad-Port Antennas Based on a Varactor Diode for Sub-6 GHz 5G Communications," *Progress in Electromagnetics Research C*, vol. 145, pp. 91-100, July 2024.

[36] A.G. Charles and Y. Guo, "A General Approach for Synthesizing Multibeam Antenna Arrays Employing Generalized Joined Coupler Matrix," *IEEE Transactions on Antennas and Propagation*, vol. 256, pp. 7556-7564, September 2022.

[37] R. Wanying, Z. Wang, M. Yang, J. Zhou and W. Nie, "Design of a Simple Four-Port UWB-MIMO Antenna Based on a Fan-Shaped Isolator," *Progress in Electromagnetics Research M*, vol. 126, pp. 117-126, April 2024.

[38] M. Saikumar, A. Fakirde and P.D. Peshwe, "Flexible Microstrip Patch Antenna Design on Jeans Substrate Radiating at 2,45 GHz for WBAN Application," *Progress in Electromagnetics Research M*, vol. 122, pp. 1-9, September 2023.

[39] H. Kazuhide, S. Tsubouchi and H. Nakano, "Series-Fed Loop Antenna Arrays with an Expanded Bandwidth of Circular Polarization," *Progress in Electromagnetics Research Letters*, vol. 114, pp. 75-81, November 2023.

[40] S.H. Ghadeer, S.K.A. Rahim, M. Alibakhshikenari, B.S. Virdee, T.A. Elwi, A. Iqbal and M.A. Hasan, "An innovative fractal monopole MIMO antenna for modern 5G applications," *AEU - International Journal of Electronics and Communications*, vol. 159, 154480, February 2023.

[41] X. Song, Y. Shen, Z. Xu, W. Wan and S. Hu, "Double-Layer Cross-Embedded Holographic Antennas with Compact Size and High Efficiency," *IEEE Transactions on Antennas and Propagation*, vol. 72, no. 7, pp. 5436-5446, May 2024.

[42] H. Feng, L. Zhu and H. Zhang, "Study on a Multi-Point Differential Feeding Strategy for Design of Filtering Patch Antennas with Stopband Enhancement," *IEEE Transactions on Antennas and Propagation*, vol. 70, no. 12, pp. 11293-11300, September 2022.